Machine learning-based CT radiomics model Distinguishes COVID-19 from other viral pneumonia

Hui Juan Chen
Department of Radiology, Hainan General Hospital (Affiliated Hainan Hospital of Hainan Medical College)
Yang Chen
Department of Radiology, Hainan General Hospital (Affiliated Hainan Hospital of Hainan Medical College)
Li Yuan
Department of Radiology, Hainan General Hospital (Affiliated Hainan Hospital of Hainan Medical College)
Fei Wang
Department of Radiology, Hainan General Hospital (Affiliated Hainan Hospital of Hainan Medical College)
Li Mao
Deepwise AI Lab, Deepwise Inc., No. 8 Haidian avenue, Sinosteel International Plaza
Xiuli Li
Deepwise AI Lab, Deepwise Inc., No. 8 Haidian avenue, Sinosteel International Plaza
Qinlei Cai
Department of Radiology, Hainan General Hospital (Affiliated Hainan Hospital of Hainan Medical College)
Jie Qiu
Department of Ultrasound, Hainan General Hospital (Affiliated Hainan Hospital of Hainan Medical College)
Jie Tian
Director of CAS Key Laboratory of Molecular Imaging, Institute of Automation, Chinese Academy of Science
Feng Chen (fenger0802@163.com)
Department of Radiology, Hainan General Hospital (Affiliated Hainan Hospital of Hainan Medical College)

Research Article

Keywords: Machine learning, radiomics, Coronavirus Disease 2019 (COVID-19), viral pneumonia

Posted Date: June 1st, 2020

DOI: https://doi.org/10.21203/rs.3.rs-32511/v1

Abstract

Purpose To develop a machine learning-based CT radiomics model is critical for the accurate diagnosis of the rapid spread Coronavirus disease 2019 (COVID-19).

Methods In this retrospective study, a machine learning-based CT radiomics model was developed to extract features from chest CT exams for the detection of COVID-19. Other viral-pneumonia CT exams of the corresponding period were also included. The radiomics features extracted from the region of interest (ROI), the radiological features evaluated by the radiologists, the quantity features calculated by the AI segmentation and evaluation, and the clinical parameters including clinical symptoms, epidemiology history and biochemical results were enrolled in this study. The SVM model was built and the performance on the testing cohort was evaluated by the area under the receiver operating characteristic curve (AUC), sensitivity and specificity.

Results For the SVM model that built on the radiomics features only, it reached an AUC of 0.688(95% CI 0.496 to 0.881) on the testing cohort. After the radiological features were enrolled, the AUC achieved 0.696(95% CI 0.501 to 0.892), then the AUC reached 0.753(95% CI 0.596 to 0.910) after the quantity features were included. Our final model employed all the features, reached the per-exam sensitivity and specificity for differentiating COVID-19 was 29 of 38 (0.763, 95% CI: 0.598 to 0.886]) and 12 of 13 (0.923, 95% CI: 0.640 to 0.998]), respectively, with an AUC of 0.968(95% CI 0.911 to 1.000).

Conclusion The machine learning-based CT radiomics models may accurately detect COVID-19 and differentiate it from other viral pneumonia.

Introduction

The Coronavirus Disease 2019 (COVID–19) has widely and rapidly spread throughout the world since late December 2019[1, 2]. The newly emerging disease is highly contagious and may cause severe acute respiratory distress or multiple organ failure in severe cases [3–6]. The World Health Organization (WHO) declared the outbreak of COVID–19 as a “public health emergency of international concern” (PHEIC) on January 30, 2020.

At present, the gold standard for the diagnosis of COVID–19 is reverse-transcription polymerase chain reaction (RT-PCR). However, a high false negative rate [7] and the shortage of RT-PCR assay in the early stage of the outbreak limited the early detection and treatment of the presumptive patients [8, 9]. This speeded up the spread of COVID–19. Therefore, fast diagnosis is important for controlling the spread of COVID–19. Recent studies have demonstrated that computed tomography (CT), as a non-invasive imaging approach, is of great value in detecting lung lesions in patients with COVID–19 infection [2, 10]. Besides, CT had much higher sensitivity than initial RT-PCR in diagnosing COVID–19 [8, 9]. Consequently, CT could be used as an effective tool for early detection and diagnosis of COVID–19. We should not neglect the fact that COVID–19 may have certain similar CT imaging features with other types of pneumonia, thus making it hard to differentiate.

Current studies have demonstrated that artificial intelligence could distinguish COVID–19 from other pneumonia [11, 12], improve radiologists’ performance in distinguishing COVID–19 from non-COVID–19 pneumonia on chest CT and provide clinical prognosis with good accuracy that can assist clinicians to timely adjust their clinical management and allocate resources appropriately[13–19]. However, COVID–19 is caused by SARS-CoV–2 virus, its CT manifestations resemble other types of viruses. Most of the published works of literature have not included the viral pneumonia as the comparison group. Additionally, the non-COVID–19 diseases included as a comparison group are long before the COVID–19 outbreak. The most difficult situation in clinical diagnosis and treatment is to identify other viral pneumonias that occurred in the same period as the epidemic of COVID–19.

In recent years, much attentions had been paid to radiomics in disease diagnosis and treatment outcome evaluation [20, 21]. Specifically, radiomics is of great value in medical imaging because of its ability to extract high throughput of quantitative descriptors from routine computed tomography (CT) studies[21]. Radiomics was applied to many fields of cancer, such as tumor detection, preoperative prediction of lymph node metastasis and therapeutic response assessment [20, 22, 23]. Recently, radiomics have been proved to be helpful in COVID–19 screening, diagnosis, prediction of hospital stay, assessing the imaging characteristics and risk factors associated with adverse composite endpoints in patients with COVID–19 pneumonia [24–27]. However, these studies were limited in small sample size. In the study of Qi et al., 31 patients were finally included in the study[25]. Some did not extract high-throughput imaging features[27]. Besides, no radiomics study of COVID–19 has been done compared with other viral pneumonia of the corresponding period, which is difficult to differentiate from COVID–19. The purpose of this study was to develop and test machine learning-based CT radiomics models for the detection of COVID–19. Other viral-pneumonia exams were also included to test the robustness of the model.

Materials And Methods

Study population

This retrospective study was waived by the ethics committees of the Hainan General hospital. In total, 74 patients confirmed with COVID-19 infection from January 20 to February 8, 2020, and 73 patients with other viral pneumonia of the corresponding period were collected. In the COVID-19 dataset, 66 patients were finally included who met the following inclusion criteria: (i) RT-PCR confirmed COVID-19; (ii) non-contrast CT at diagnosis time; (iii) positive CT findings. Other viral pneumonias were included who met the following inclusion criteria: (i) RT-PCR excluded COVID-19; (ii) non-contrast CT at diagnosis time; (iii) viral pneumonia highly suspected with COVID-19 at CT. The exclusion criteria were as follows: 1) contrast CT exam; 2) exams without slice thickness of 1mm; 3) negative CT findings. Finally, 326 chest CT exams from 137 patients were included in this study (**Fig. 1**). The average age is 47.0±15.4 years. Finally, we included 244 (75%) exams for COVID-19 and 82(25%) for other viral pneumonia in the study.

All the COVID-19 were confirmed as positive by RT PCR and were acquired from January 21, 2020, to Feb 8, 2020. The most common symptoms were fever (82%) and cough (77%). Each patient had one or multiple CT scans during the progression of the disease. The follow-up study was performed until February 19,2020.

Other viral-pneumonia patients were selected from the hospital of the corresponding period between January 23 to March 16, 2020. The admission distribution of the patients with other viral-pneumonia was: outpatient (86%, 61 of 71), inpatient (14%, 10 of 71). No one received laboratory confirmation of the etiology because of limited medical resources.
All the CT scans were split with a ratio of 85:15 into a training cohort and a testing cohort at the patient level according to the visiting time of the hospital. The features selection and model building were performed on the training cohort, and the testing cohort was not used for the training procedure. The patient demographic statistics are summarized in Table 1.

Imaging Protocol

CT examinations were performed on the NeuViz 128 CT (Neusoft, China) with automatic tube current (300 mA-496 mA). The pitch was set at 1.5 and breath-hold at full inspiration. The slice-thickness of each CT scan was 1mm. The reconstruction matrix was 512x512 pixels. The flow chart of data collection, ROI and features annotation, radiomics and quantity feature extraction, model building and evaluation are shown in **Fig. 2**.

Lesion segmentation and radiological evaluation

The anonymized thin-slice DICOM format non-enhanced CT images were imported into the Dr. Wise research platform, on which the pneumonia lesions were automatically delineated by deep-learning segmentation algorithms. Fifteen radiologists with more than 5 years of experience in chest imaging, blind to the knowledge of the pathological report and other clinical information, confirmed the segmentation result (Region of Interest, ROI) and evaluated the radiological characteristics. The segmentations and radiological characteristics were confirmed by two radiologists (F. C and Y.C) with 16 and more than 30 years of experience.

The 7 radiological characteristics included ground grass opacity, crazy paving pattern, halo sign, reversed halo sign, vascular perforating in the lesion, subpleural line and lesion locations (**Fig. 3**). For each series, the frequency of the radiological characteristics occurring was used for modeling.

Quantitative CT characteristics and radiomics features

The segmentation result was used to extract quantitative CT characteristics and radiomics features. The delineation of the pulmonary lobes was segmented by the Dr. Wise research platform and the lesion and lobe information were extracted to construct quantitative characteristics of pneumonia.

There were a total of 33 quantitative characteristics, including the volume of the lesions, mean and standard deviation of the CT values in lesions, consolidation lesions and ground glass lesions respectively, the number of the consolidation lesions and the number of the ground glass lesions, the ratio of the volume of these lesions in the entire pulmonary and the five pulmonary lobes respectively, and the number of lesions that suffered bulla, emphysema, pleural thickening, reticular, and stripe.

Before the radiomics features were extracted, the pixel spacing of images was resampled to 1.0 mm per pixel by the BSpline algorithm. Besides the original images, the wavelet filters or Laplacian of Gaussian filters were performed to generate several filtered images. A total of 1218 radiomics features were extracted from the manual confirmed ROIs of the original images and the filtered images by PyRadiomics V2.1.0, including (1) 252 First-order features; (2) 14 Shape-based features; (3) 308 Gray Level Co-occurrence Matrix Features (GLCM); (4) 224 Gray Level Size Zone Matrix Features (GLSZM); (5) 224 Gray Level Run Length Matrix Features (GLRLM); (6) 196 Gray Level Dependence Matrix Features (GLD-ZM). The pre-processing methods and radiomic feature descriptions are detailed in **Supplementary Information 1.1.** and **1.2**.

Development of predictive models

The features were stacked in the order of radiomics features, radiological features，quantity features and clinical features, and 4 SVM models with radial basis function kernel were built. All numerical features were normalized to [0,1], and the categorical features were encoded by one-hot

encoder. To avoid overfitting, the feature selection methods were used to reduce the dimension of the features. The optimal parameters of the combination of the feature selection method and the model were found by grid search using a ten-run 5-fold cross validation procedure on the training cohort. After the optimal params were determined, the entire training cohort was used to build the model and the performance on the testing cohort was evaluated. After the cross-validation procedure, the threshold that maximum the Youden Index was used to cut-off the discriminative score to differentiate the COVID-19 from other virus pneumonia. The evaluation indicators include the area under the receiver operator characteristic curve (AUC), accuracy (ACC), sensitivity and specificity.

The feature selection method we used included the f-test based method and the L1 based method. The f-test based feature selection method with different preserve ratio (1%, 5%, 10%, 30%, 50% and 100%) were tested, while the L1 based method that used linear C-support vector classification model with different C value (0.01, 0.1, 1, and 10) as a base model was tested.

Results

Table 1 demonstrates the study population characteristics for the training and testing cohorts. There are slightly more male patients than female patients across COVID-19 and other viral-pneumonia groups for both training cohort (gender: COVID-19: 61%; Other viral-pneumonia: 55%) and testing cohort (gender: COVID-19: 50%; Other viral-Pneumonia: 73%). Patients with COVID- 19 are older than the ones in the other viral-pneumonia group for the training cohort (age: COVID-19: 52.9; Other viral-pneumonia: 41.5; p-value<0.001). The most common symptoms for COVID-19 and other viral pneumonia was a fever for the training cohort (fever: COVID-19: 87%; Other viral-pneumonia: 77%) and testing cohort (58%;64%).The white blood cell count and neutrophils of patients with COVID- 19 are lower than the ones in the other viral-pneumonia group for the training cohort (white blood cell count: COVID-19: 4.8; Other viral-pneumonia: 8.2; p-value<0.001. neutrophils: COVID-19: 3.2; Other viral-Pneumonia: 5.8; p-value<0.001) and testing cohort (white blood cell count: COVID-19: 5.4; Other viral-Pneumonia: 9.4; p-value=0.002; neutrophils: COVID-19: 3.4; Other viral-pneumonia: 6.8; p-value=0.005). The lymphocyte and platelet count of patients with COVID- 19 are lower than the ones in the other viral-pneumonia group for the training cohort (lymphocyte count: COVID-19: 1.2; Other viral-pneumonia: 1.6; p-value=0.039. platelet count: COVID-19: 176.0; Other viral-pneumonia: 225.6; p-value<0.001)

Table 1. Characteristics of Patients in the training and testing Cohorts

Characteristic	Training cohort			testing cohort		
	COVID-19	Other Viral-pneumonia	P value	COVID-19	Other viral-pneumonia	p Value
Patients	54	60	-	12	11	-
Exams	206	69	-	38	13	-
Age	52.9±12.5	41.5±15.5	<0.001[b]	47.7±15.3	46.9±18.4	0.915[b]
Gender,Male(%)	33(61%)	33(55%)	0.509[a]	6(50%)	8(73%)	0.247[a]
Clinical types			0.016[c]			1.000[c]
Mild	0(0%)	0(0%)		0(0%)	0(0%)	
Common	46(85%)	59(98%)		12(100%)	11(100%)	
Severe	2(4%)	1(2%)		0(0%)	0(0%)	
Critical	5(9%)	0(0%)		0(0%)	0(0%)	
Exposure history			<0.001[c]			0.340[c]
Working or study in Wuhan	41(76%)	22(37%)		0(0%)	1(9%)	
Travel to Wuhan	1(2%)	6(10%)		2(17%)	0(0%)	
Close contact with infected patients	12(22%)	25(42%)		7(58%)	5(45%)	
Unknown cause	0(0%)	8(13%)		3(25%)	5(45%)	
Comorbidities, No. (%)			-			-
Cardiovasular disease	1(2%)	1(2%)	1.000[a]	2(17%)	1(9%)	1.000[a]
Diabetes	5(9%)	0(0%)	0.051[a]	0(0%)	0(0%)	-
Hypertension, No. (%)	9(17%)	4(7%)	0.093[a]	0(0%)	1(9%)	0.478[a]
COPD	3(6%)	2(3%)	0.904[a]	0(0%)	0(0%)	-
Chronic liver disease	3(6%)	1(2%)	0.537[a]	0(0%)	0(0%)	-
Chronic kidney disease	0(0%)	0(0%)	-	0(0%)	1(9%)	0.478[a]
Cancer, No. (%)	0(0%)	1(2%)	1.000[a]	0(0%)	2(18%)	0.217[a]
Symptoms						
Fever, No. (%)	47(87%)	46(77%)	0.154[a]	7(58%)	7(64%)	0.795[a]
Cough, No. (%)	44(81%)	26 (43%)	**<0.001**[a]	7(58%)	3(27%)	0.280[a]
Myalgia, No. (%)	10(19%)	2(3%)	0.008[a]	2(17%)	0(0%)	0.478[a]
Fatigue, No. (%)	18(33%)	2(3%)	<0.001[a]	0(0%)	0(0%)	-
Headache, No. (%)	9(17%)	1(2%)	0.013[a]	2(17%)	0(0%)	0.478[a]
Nausea, No. (%)	5(9%)	0(0%)	0.051[a]	2(17%)	0(0%)	0.478[a]
Diarrhea, No. (%)	7(13%)	1(2%)	0.047[a]	1(8%)	0(0%)	1.000[a]
bellyache, No. (%)	0(0%)	0(0%)	-	1(8%)	0(0%)	1.000[a]
Dyspnea, No. (%)	1(2%)	0(0%)	0.474[a]	0(0%)	0(0%)	-
Other symptoms, No. (%)	19(35%)	14(23%)	0.164[a]	5(42%)	2(18%)	0.442[a]
Laboratory results						
White blood cell count	4.8±2.0	8.2±3.5	**<0.001**[b]	5.4±1.9	9.4±3.4	**0.002**[b]
Number of neutrophils, × 10⁹/L	3.2±1.9	5.8±3.2	**<0.001**[b]	3.4±1.7	6.8±3.3	**0.005**[b]
Lymphocyte count, ×10⁹/L	1.2±0.8	1.6±1.1	**0.039**[b]	1.4±0.5	1.7±1.0	0.360[b]
Hemoglobin	133.4±24.9	138.7±17.6	0.198[b]	127.4±19.1	139.7±21.3	0.159[b]
Platelet count, ×10⁹/L	176.0±59.2	225.6±62.0	**<0.001**[b]	213.7±67.7	230.1±89.0	0.622[b]
Treatment						
Hospitalization	54(100%)	8(13%)	<0.001[a]	12(100%)	2(18%)	<0.001[a]
ICU	5(9%)	0(0%)	0.022[a]	0(0%)	0(0%)	-
mechanical ventilation	6(11%)	0(0%)	0.027[a]	0(0%)	0(0%)	-
Prognosis						
Discharged	53(98%)	8(13%)	-	12(100%)	1(9%)	-
Death	1(2%)	0(0%)	-	0(0%)	0(0%)	-

p[a] : chi-square test, p[b] : Student's t test. p[c] : Kruskal-Wallis H test

Evaluation of the model performance

A total of 1128 features were extracted from each patient, represented on the correlation cluster map shown in **Fig. 4**. For the SVM model that built on the radiomics features only (R model, Radiomic), it reached an AUC of 1.000 (95% CI 1.000 to 1.000), 0.907(95% CI 0.864 to 0.951), and 0.688(95% CI 0.496 to 0.881) on the training, cross-validation and testing cohort. For the sensitivity and specificity, it reached both 1.000 on the training cohort, 0.859 and 0.870 on the cross-validation cohort and 0.526 and 0.769 on the test cohort. After the radiological features were enrolled (RR model, Radiomics & radiological features), the AUC on the testing cohort achieved 0.696 (95% CI 0.501 to 0.892). The AUC on the testing cohort reached 0.753(95% CI 0.596 to 0.910) after the quantity features were included (RRQ model, Radiomics & radiological features & quantity features).

There was a significant improvement in the performance of the SVM model after the clinical features were enrolled (RRQC model, Radiomics & radiological features & quantity features & clinical features). The AUC reached 0.999 (95% CI 0.996 to 1.000), 0.979 (95% CI 0.961 to 0.997) and 0.968(95% CI 0.911 to 1.000) on the training, cross-validation and testing cohort. For the sensitivity and specificity, it reached 0.995 and 0.928 on the training cohort, 0.961 and 0.899 on the cross-validation cohort and 0.763 and 0.923 on the test cohort.

The details of the performance are shown in table 2 and the ROC curve of the 4 SVM models was shown in **Fig. 5**. The ridgeline plot (**Fig. 6**) showed the distribution of the normalized features selected for RRQC by our feature selection strategy, only numerical features were shown in this plot. Two image features, 2 biochemical indexes, 5 shape-based radiomics features, 2 intensity-based features and 1 texture feature on images preprocessed by wavelet filter were preserved.

Table 2. The performance of CT radiomics models in training, inter-validation and testing cohorts.

Models		AUC(95% CI)	ACC (95% CI)	Specificity(95% CI)	Sensitivity (95% CI)
R model	training	1.000(1.000 to 1.000)	1.000(0.987 to 1.000)	1.000(0.948 to 1.000)	1.000(0.982 to 1.000)
	validation	0.907(0.864 to 0.951)	0.862(0.815 to 0.900)	0.870(0.767 to 0.939)	0.859(0.804 to 0.904)
	testing	0.688(0.496 to 0.881)	0.588(0.442 to 0.724)	0.769(0.462 to 0.950)	0.526(0.358 to 0.69)
RR model	training	1.000(1.000 to 1.000)	1.000(0.987 to 1.000)	1.000(0.948 to 1.000)	1.000(0.982 to 1.000)
	validation	0.924(0.886 to 0.962)	0.847(0.799 to 0.888)	0.913(0.820 to 0.967)	0.825(0.766 to 0.874)
	testing	0.696(0.501 to 0.892)	0.608(0.461 to 0.742)	0.769(0.462 to 0.950)	0.553(0.383 to 0.714)
RRQ model	training	1.000(1.000 to 1.000)	1.000(0.987 to 1.000)	1.000(0.948 to 1.000)	1.000(0.982 to 1.000)
	validation	0.946(0.916 to 0.975)	0.895(0.852 to 0.928)	0.841(0.733 to 0.918)	0.913(0.865 to 0.947)
	testing	0.753(0.596 to 0.910)	0.667(0.521 to 0.792)	0.615(0.316 to 0.861)	0.684(0.513 to 0.825)
RRQC	training	0.999(0.996 to 1.000)	0.978(0.953 to 0.992)	0.928(0.839 to 0.976)	0.995(0.973 to 1.000)
	validation	0.979(0.961 to 0.997)	0.945(0.912 to 0.969)	0.899(0.802 to 0.958)	0.961(0.925 to 0.983)
	testing	0.968(0.911 to 1.000)	0.804(0.669 to 0.902)	0.923(0.640 to 0.998)	0.763(0.598 to 0.886)

R, RR, RRQ and RRQC models indicate the predicted model based on radiomics feature, radiomics & radiological features, radiomics & radiological & quantity features and the combination of radiomics & radiological & quantity & clinical features, respectively. . CI confidence interval

For the RRQC model, **Fig. 7** showed the decision function value distribution of the other viral pneumonia and COVID-19 in the test cohort. The function values are proportional to the distance of the patient to the separating hyperplane, thus indicate the model's confidence in the result of classification. The separating hyperplane was adjusted to maximize the Youden index on the training cohort. From the CT images, we could see that when the lesions of COVID-19 were at absorption stage, it became small and thus it is difficult to differentiate from other viral pneumonia. On the contrary, when the lesions of COVID-19 were relatively big, it is easy to differentia it from other viral pneumonia with typical lesion locations and CT manifestation.

Discussion

In this study, we developed and tested a machine learning-based CT radiomics model for detecting COVID-19 from chest CT images. CT radiomics features of lesions were extracted, and machine-learning model showed good performance for training, inter-validation and testing cohort. On the testing dataset, our result revealed that this model achieved high sensitivity (0.763, 95% CI: 0.598 to 0.886) and high specificity of (0.923, 95% CI: 0.640 to 0.998) in diagnosing COVID-19. The AUC values for COVID-19 and other viral pneumonia were 0.968 (95% CI 0.911 to 1.000).

The encouraging diagnostic performance of the machine learning-based CT radiomics model indicates that radiomics may be helpful for the detection of COVID-19. Radiomics features in our model included first order features, shape-based features and the distribution, correlation and variance in gray level intensities. These radiomics features described the relationship between voxels and contained quantitative information on the spatial heterogeneity of pneumonia lesions. Importantly, when radiomics features were included alone, the model revealed the good performance of AUCs for training, validation and testing cohort, 100%, 90.7%and 68.8%, respectively. After including the subjective features, quantitative characteristics and clinical characteristics, the performance of the model was gradually improved. The model demonstrated satisfied AUCs more than 95% on training, validation and testing cohorts, indicating that the models have the potential to be applied in a general situation. By using deep learning techniques, previous study was able to distinguish COVID-19 from community acquired pneumonia[11]. We were able to collect a number of patients with viral pneumonia diagnosis on CT of the corresponding period. More importantly, these pneumonia were highly suspected of COVID-19 in consideration of the epidemic, CT findings, and laboratory results.

A majority of the countries all over the world have been affected by COVID-19. Early diagnosis is of importance for preventing the spread of the disease. Though RT-PCR is considered as the gold standard for the diagnosis of COVID-19, CT is used as an effective supplementary tool for the diagnosis of COVID-19 [8, 9]. Our study revealed that the machine learning-based CT radiomics model by combining radiomics, subjective characteristics, quantitative characteristics and clinical characteristics achieved good performance for the diagnosis of COVID-19 and differentiating it from other viral pneumonia.

Limitations

The study has several limitations. First, the sample size was relatively small. A larger prospective multicenter cohort is needed to test the effectiveness of machine learning-based CT radiomics models. Second, patients with other viral pneumonia did not receive laboratory confirmation of the etiology because of limited medical resources during the COVID-19 outbreak. Thirdly, we did not use quantitative characteristics to evaluate the evolution of the disease. Future work should include quantitative information regarding disease progression.

Conclusion

In conclusion, a machine learning-based CT radiomics model is valuable for accurately detecting COVID-19 and differentiating it other pneumonia from chest CT images.

Declarations

Authors' contributions JT, and FC designed the study; HJC was a major contributor in writing the manuscript; YC, YL, FW, ML, XL, QL, JQ collected the imaging and clinical data; HJC, YC, YL, FW, ML, XL, QL, JQ, JT, and FC revised it critically for important intellectual content. All authors have read and approved the manuscript.

Compliance with ethical standards

Conflict of interest The authors declare that they have no conflicts of interest.

Ethics approval/consent to participate The study was conducted in line with the principles of the Declaration of Helsinki, and Institutional Review Board approval has been obtained. The written informed consent for this retrospective study was waived

Funding This work was supported by the Key R & D plan of Hainan Province (ZDYF (XGFY) 2020001) ; National Nature Science Foundation of China [grant number 81971602, 81760308, 81801684, 81871346]; the Program of Hainan Association for Science and Technology Plans to Youth R & D Innovation [QCXM201919]; Hainan Provincial Natural Science Foundation of China [818MS124].

References

1. Wang D, Hu B, Hu C, Zhu F, Liu X, Zhang J, et al. Clinical Characteristics of 138 Hospitalized Patients With 2019 Novel Coronavirus-Infected Pneumonia in Wuhan, China. Jama. 2020. doi:10.1001/jama.2020.1585.
2. Huang C, Wang Y, Li X, Ren L, Zhao J, Hu Y, et al. Clinical features of patients infected with 2019 novel coronavirus in Wuhan, China. Lancet (London, England). 2020. doi:10.1016/s0140-6736(20)30183-5.
3. Chen N, Zhou M, Dong X, Qu J, Gong F, Han Y, et al. Epidemiological and clinical characteristics of 99 cases of 2019 novel coronavirus pneumonia in Wuhan, China: a descriptive study. Lancet (London, England). 2020;395:507-13. doi:10.1016/s0140-6736(20)30211-7.
4. Phan LT, Nguyen TV, Luong QC, Nguyen TV, Nguyen HT, Le HQ, et al. Importation and Human-to-Human Transmission of a Novel Coronavirus in Vietnam. The New England journal of medicine. 2020;382:872-4. doi:10.1056/NEJMc2001272.
5. Liu YC, Liao CH, Chang CF, Chou CC, Lin YR. A Locally Transmitted Case of SARS-CoV-2 Infection in Taiwan. The New England journal of medicine. 2020;382:1070-2. doi:10.1056/NEJMc2001573.
6. Li Q, Guan X, Wu P, Wang X, Zhou L, Tong Y, et al. Early Transmission Dynamics in Wuhan, China, of Novel Coronavirus-Infected Pneumonia. The New England journal of medicine. 2020. doi:10.1056/NEJMoa2001316.
7. Chan JF, Yuan S, Kok KH, To KK, Chu H, Yang J, et al. A familial cluster of pneumonia associated with the 2019 novel coronavirus indicating person-to-person transmission: a study of a family cluster. Lancet (London, England). 2020. doi:10.1016/s0140-6736(20)30154-9.
8. Ai T, Yang Z, Hou H, Zhan C, Chen C, Lv W, et al. Correlation of Chest CT and RT-PCR Testing in Coronavirus Disease 2019 (COVID-19) in China: A Report of 1014 Cases. Radiology. 2020:200642. doi:10.1148/radiol.2020200642.
9. Fang Y, Zhang H, Xie J, Lin M, Ying L, Pang P, et al. Sensitivity of Chest CT for COVID-19: Comparison to RT-PCR. Radiology. 2020:200432. doi:10.1148/radiol.2020200432.
10. Shi H, Han X, Jiang N, Cao Y, Alwalid O, Gu J, et al. Radiological findings from 81 patients with COVID-19 pneumonia in Wuhan, China: a descriptive study. The Lancet Infectious diseases. 2020. doi:10.1016/s1473-3099(20)30086-4.
11. Li L, Qin L, Xu Z, Yin Y, Wang X, Kong B, et al. Artificial Intelligence Distinguishes COVID-19 from Community Acquired Pneumonia on Chest CT. Radiology. 2020:200905. doi:10.1148/radiol.2020200905.
12. Wang S, Kang B, Ma J, Zeng X, Xiao M, Guo J, et al. A deep learning algorithm using CT images to screen for Corona Virus Disease (COVID-19). medRxiv. 2020.
13. Bai HX, Wang R, Xiong Z, Hsieh B, Chang K, Halsey K, et al. AI Augmentation of Radiologist Performance in Distinguishing COVID-19 from Pneumonia of Other Etiology on Chest CT. Radiology. 2020:201491. doi:10.1148/radiol.2020201491.
14. https://www.cell.com/pb-assets/products/coronavirus/CELL_CELL-D-20-00656.pdf.
15. Dong D, Tang Z, Wang S, Hui H, Gong L, Lu Y, et al. The role of imaging in the detection and management of COVID-19: a review. IEEE reviews in biomedical engineering. 2020. doi:10.1109/rbme.2020.2990959.
16. Wang S, Zha Y, Li W, Wu Q, Li X, Niu M, et al. A Fully Automatic Deep Learning System for COVID-19 Diagnostic and Prognostic Analysis. medRxiv. 2020.
17. Chen J, Wu L, Zhang J, Zhang L, Gong D, Zhao Y, et al. Deep learning-based model for detecting 2019 novel coronavirus pneumonia on high-resolution computed tomography: a prospective study. medRxiv. 2020.
18. Shan F, Gao Y, Wang J, Shi W, Shi N, Han M, et al. Lung Infection Quantification of COVID-19 in CT Images with Deep Learning. arXiv preprint 2020;arXiv:2003.04655.

19. Gozes O, Frid-Adar M, Greenspan H, Browning P, Zhang H, Ji W, et al. Rapid AI Development Cycle for the Coronavirus (COVID-19) Pandemic: Initial Results for Automated Detection & Patient Monitoring using Deep Learning CT Image Analysis. arXiv preprint. 2020;arXiv:2003.05037.
20. Dong D, Zhang F, Zhong LZ, Fang MJ, Huang CL, Yao JJ, et al. Development and validation of a novel MR imaging predictor of response to induction chemotherapy in locoregionally advanced nasopharyngeal cancer: a randomized controlled trial substudy (NCT01245959). BMC medicine. 2019;17:190. doi:10.1186/s12916-019-1422-6.
21. Lambin P, Rios-Velazquez E, Leijenaar R, Carvalho S, van Stiphout RG, Granton P, et al. Radiomics: extracting more information from medical images using advanced feature analysis. European journal of cancer (Oxford, England : 1990). 2012;48:441-6. doi:10.1016/j.ejca.2011.11.036.
22. Huang YQ, Liang CH, He L, Tian J, Liang CS, Chen X, et al. Development and Validation of a Radiomics Nomogram for Preoperative Prediction of Lymph Node Metastasis in Colorectal Cancer. Journal of clinical oncology : official journal of the American Society of Clinical Oncology. 2016;34:2157-64. doi:10.1200/jco.2015.65.9128.
23. Dong D, Tang L, Li ZY, Fang MJ, Gao JB, Shan XH, et al. Development and validation of an individualized nomogram to identify occult peritoneal metastasis in patients with advanced gastric cancer. Annals of oncology : official journal of the European Society for Medical Oncology. 2019;30:431-8. doi:10.1093/annonc/mdz001.
24. Chen X, Tang Y, Mo Y, Li S, Lin D, Yang Z, et al. A diagnostic model for coronavirus disease 2019 (COVID-19) based on radiological semantic and clinical features: a multi-center study. European radiology. 2020. doi:10.1007/s00330-020-06829-2.
25. Qi X, Jiang Z, Yu Q, Shao C, Zhang H, Yue H, et al. Machine learning-based CT radiomics model for predicting hospital stay in patients with pneumonia associated with SARS-CoV-2 infection: A multicenter study. medRxiv. 2020.
26. Fang M, He B, Li L, Dong D, Yang X, Li C, et al. CT radiomics can help screen the coronavirus disease 2019 (COVID-19): a preliminary study. SCIENCE CHINA Information Sciences. 2020;63:172103. doi:https://doi.org/10.1007/s11432-020-2849-3.
27. Yu Q, Wang Y, Huang S, Liu S, Zhou Z, Zhang S, et al.
Multicenter cohort study demonstrates more consolidation in upper lungs on initial CT increases the risk of adverse clinical outcome in COVID-19 patients. Theranostics. 2020;10:5641-8. doi:doi: 10.7150/thno.46465. eCollection 2020.

Figures

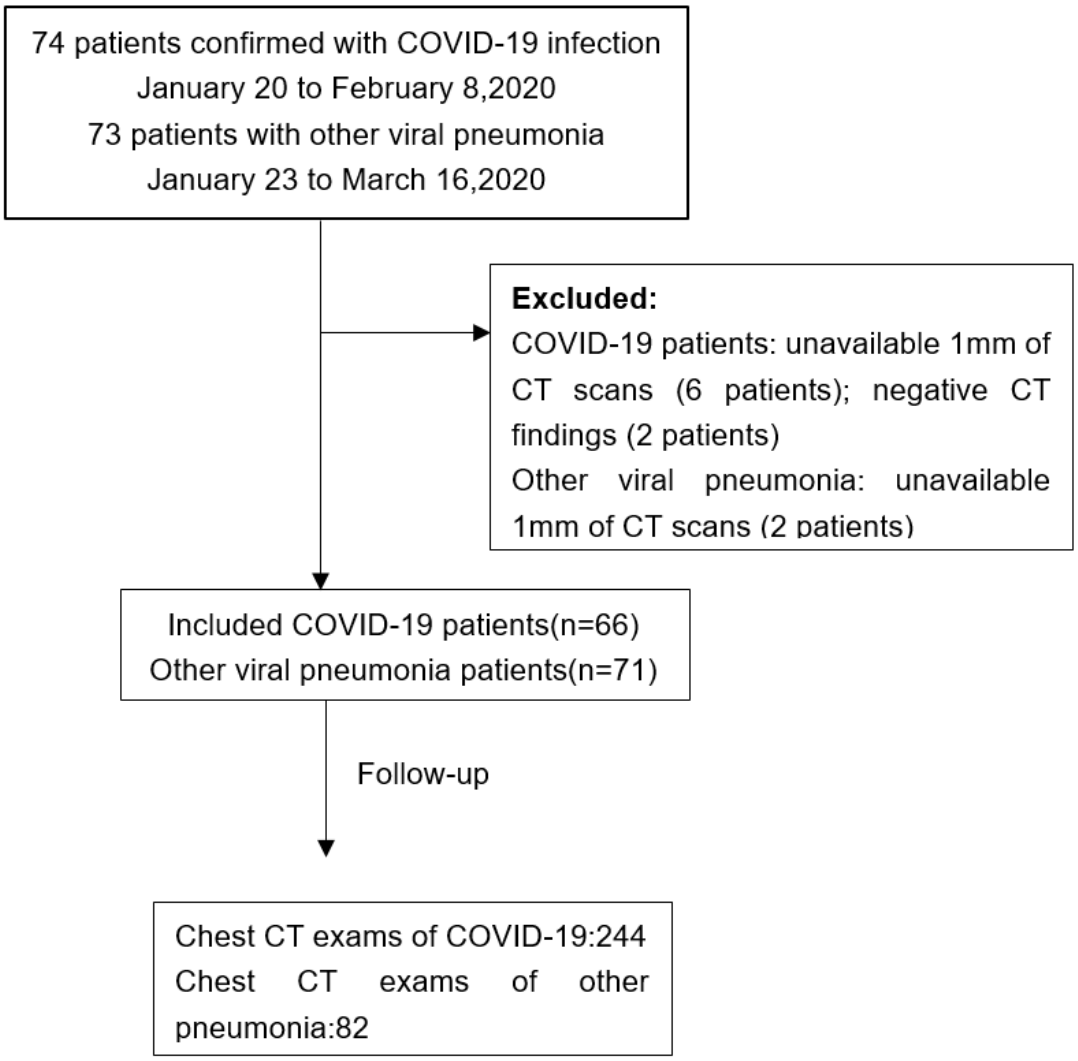

Figure 1

Flowchart of this study.

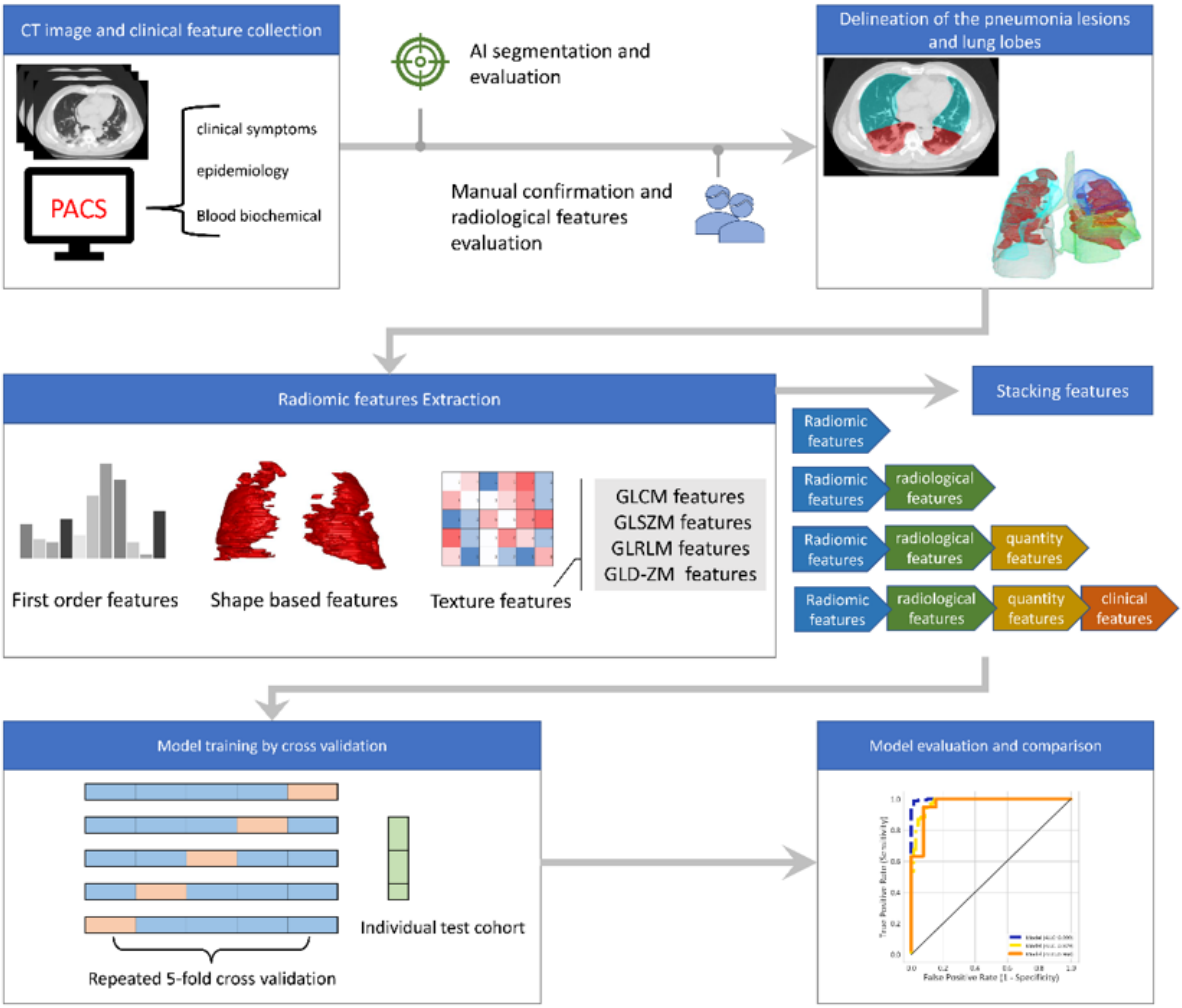

Figure 2

The flow chart showed our study workflow, consisting of data collection, ROI and features annotation, radiomic and quantity features extraction, model building and evaluation.

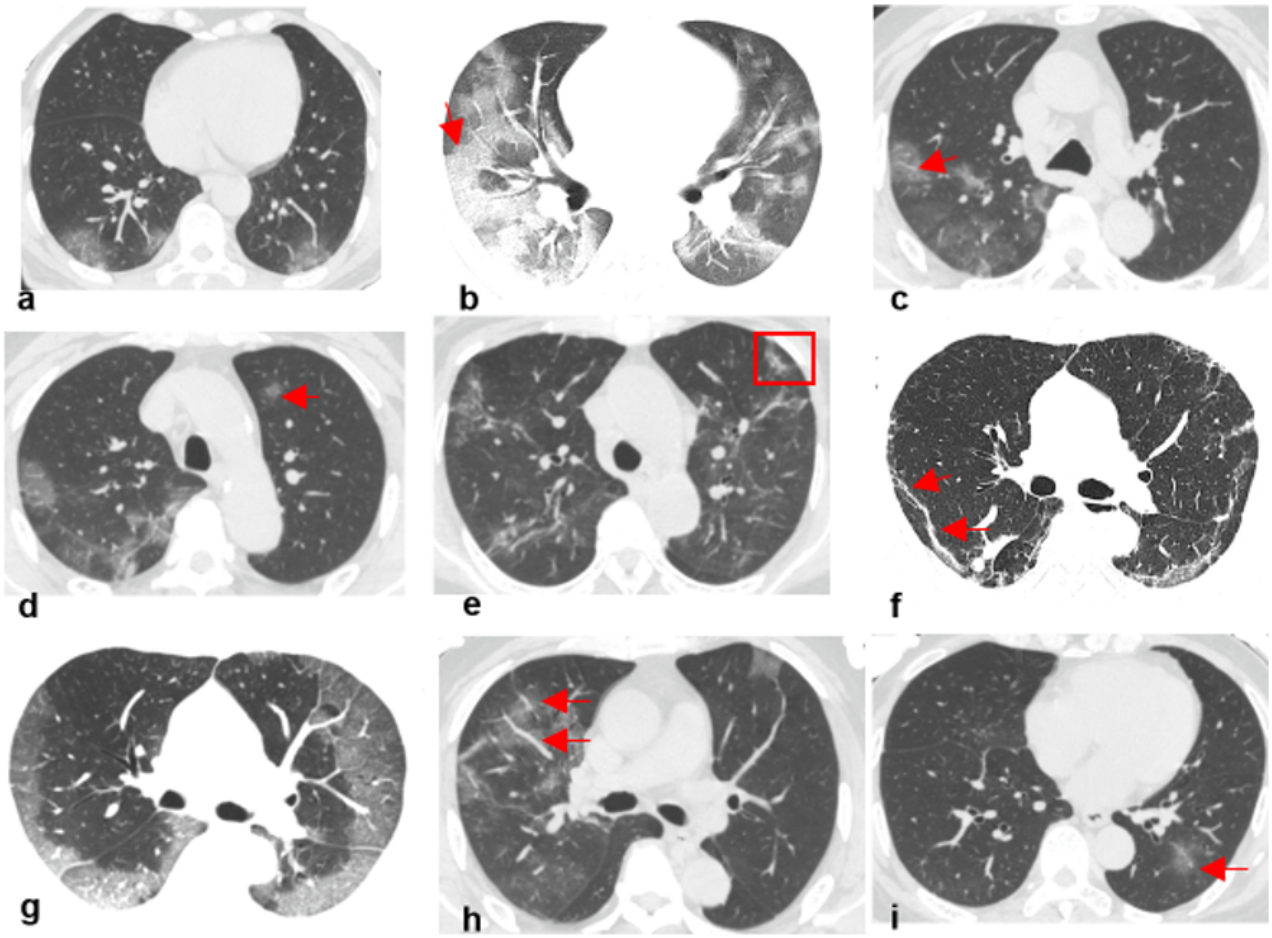

Figure 3

a-i demonstrated the typical radiological characteristics of ground grass opacity, crazy paving pattern, halo sign, reversed halo sign, vascular perforating in the lesion, subpleural line, subpleural distribution, bronchovascular bundle distribution and pulmonary band distribution, respectively.

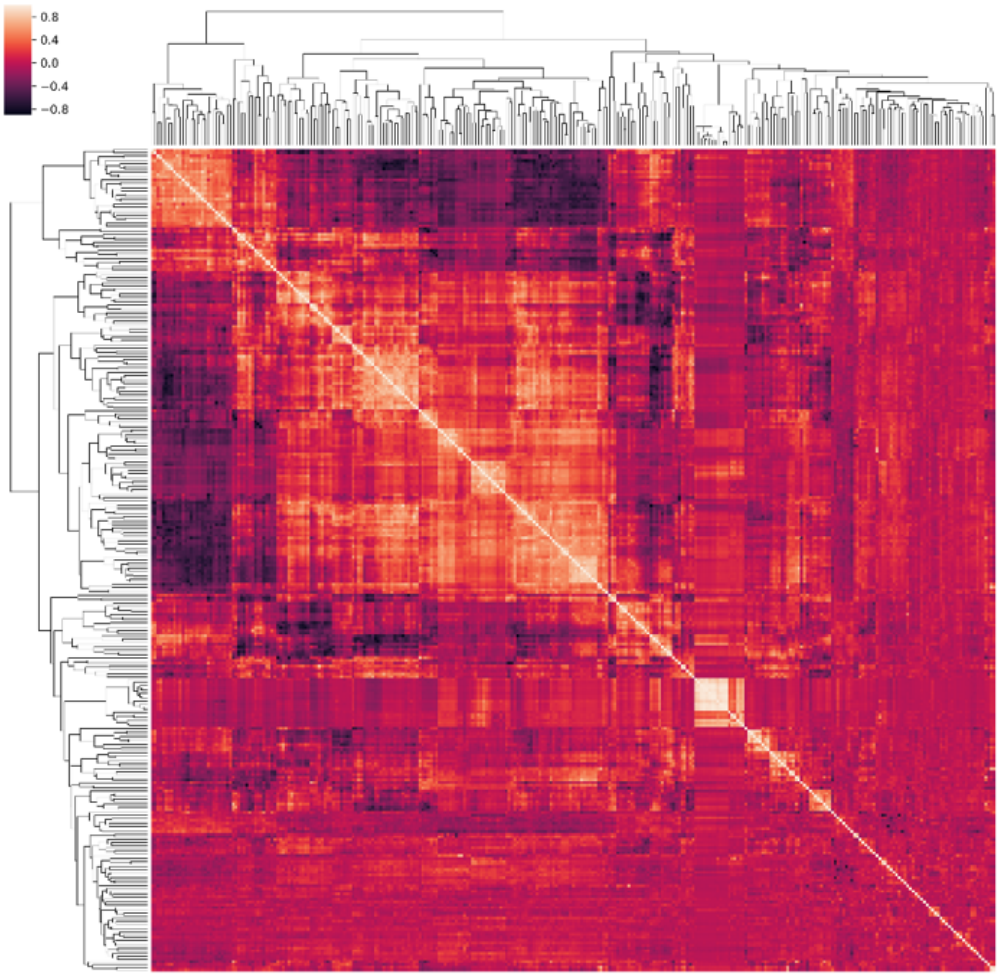

Figure 4

Feature correlation matrix represented as a hierarchically clustered heatmap

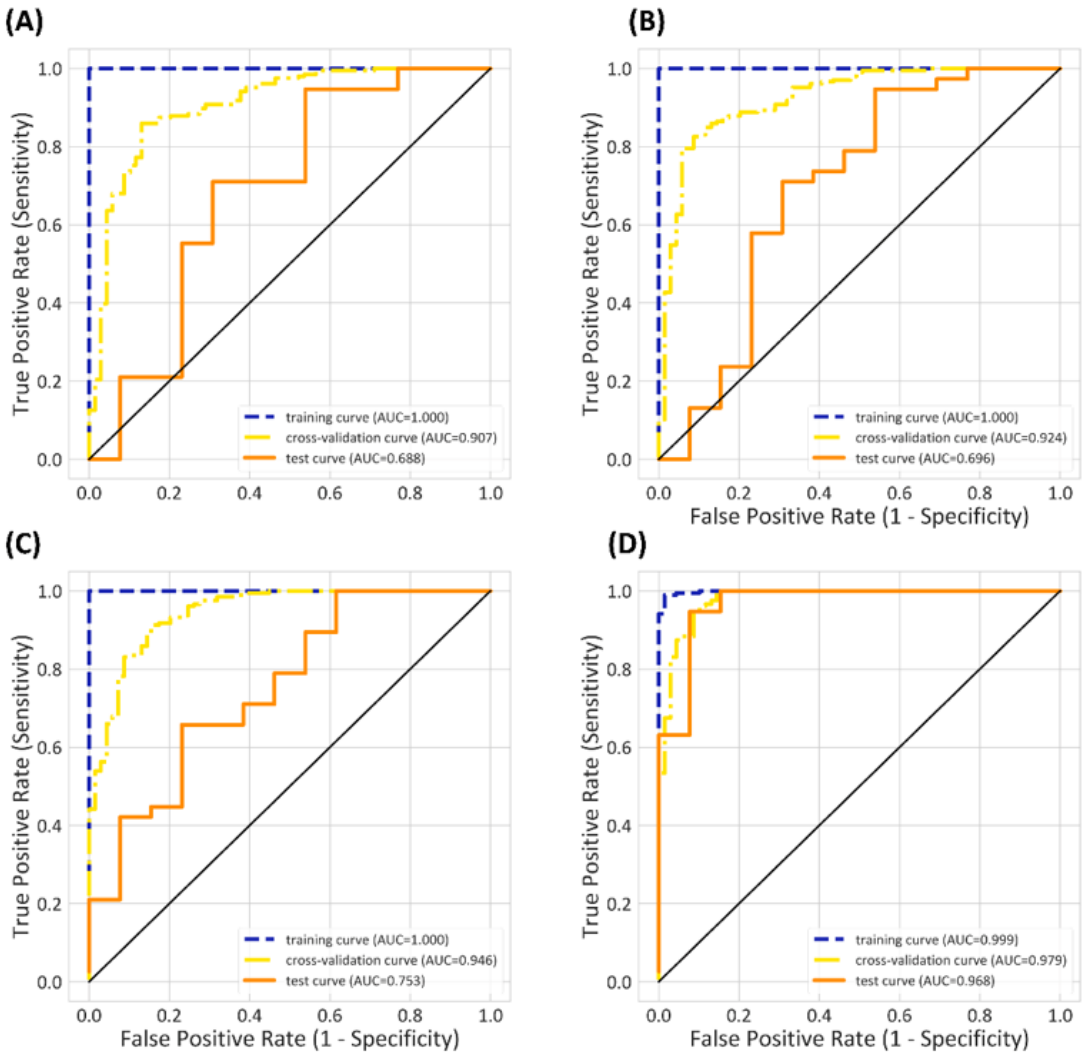

Figure 5

The training, cross-validation and testing ROC curve of R model (A), RR model (B), RRQ model (C) and RRQC model (D). The ROC curve showed the change of the sensitivity value with 1 minus specificity value under different thresholds. R, RR, RRQ and RRQC models indicate the predicted model based on radiomics feature, radiomics & radiological features, radiomics & radiological & quantity features and the combination of radiomics & radiological & quantity & clinical features, respectively.

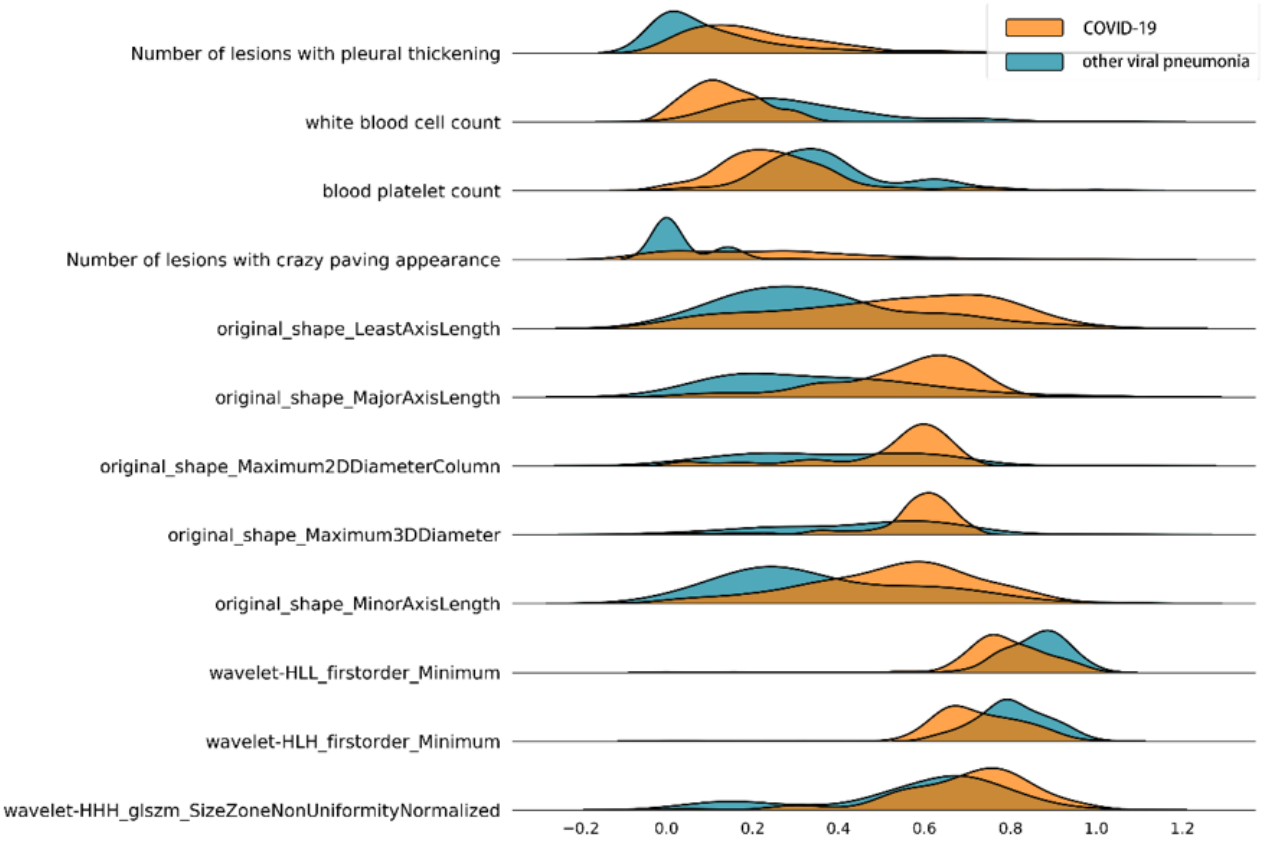

Figure 6

The ridgeline plot showed the distribution of the normalized numeric features that selected for RRQC model by our feature selection strategy. Each distribution of the feature was described by a kernel density estimate curve based on Gaussian kernel. The different color indicated the COVID-19 cohort or other viral pneumonia cohort. RRQC = radiomics & radiological & quantity & clinical features

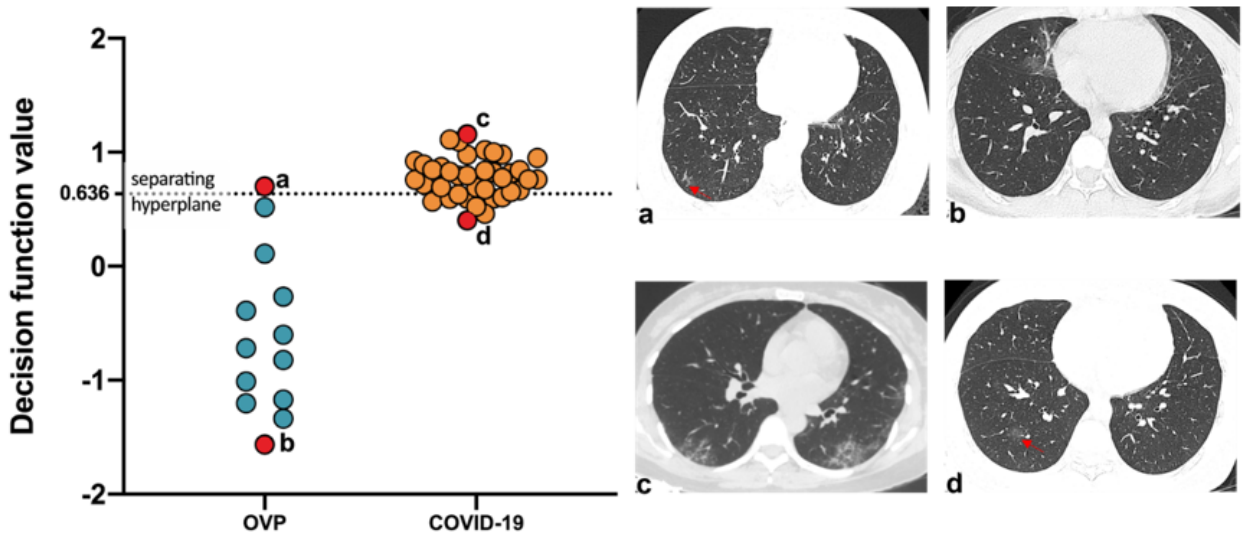

Figure 7

The decision function value distribution of the patients with Other Viral Pneumonia (OVP) and COVID-19 in the test cohort were shown. Each point indicated a patient in the test cohort, the OVP point below the adjusted separating hyperplane line and the COVID-19 point above the line were separated correctly. The images of the 4 typical patients were shown. (a) A patient with OVP that misclassified as COVID-19. (b) A patient with OVP that were correctly identified. (c) A patient with COVID-19 that were correctly identified. (d)A patient with COVID-19 that misclassified as OVP.

Supplementary Files

This is a list of supplementary files associated with this preprint. Click to download.

- Supplementarymaterial.docx